Theory for Fourier-limited attosecond pulse generation in solids

Shohei Imai [*] and Atsushi Ono

Department of Physics, Tohoku University, Sendai 980-8578, Japan

The generation of ultrashort light pulses is essential for the advancement of attosecond science. Here, we show that attosecond pulses approaching the Fourier limit can be generated through optimized optical driving of tunneling particles in solids. We propose an ansatz for the wave function of tunneling electron-hole pairs based on a rigorous expression for massive Dirac fermions, which enables efficient optimization of the waveform of the driving field. It is revealed that the dynamic sign change in the effective mass due to optical driving is crucial for shortening the pulse duration, which highlights a distinctive property of Bloch electrons that is not present in atomic gases, i.e., the periodic nature of crystals. These results show the potential of utilizing solid materials as a source of attosecond pulses.

Introduction. Ultrafast physics has advanced significantly owing to the development of femtosecond lasers [1,2]. These intense, short pulses allow for time-resolved measurements of chemical reactions of molecules [3] and even induce macroscopic phase transitions in condensed matter systems [4–7]. In recent years, the pulse duration of lasers has reached attosecond timescales, enabling observation of coherent dynamics in atoms, molecules, and solids [8–14], and potentially lightwave control of quantum systems within a single optical cycle [9,15–24], which were previously inaccessible because of relaxation and dephasing and are now attracting considerable interest.

High harmonic generation (HHG) is a phenomenon in which a series of attosecond or femtosecond pulses with broad spectra is generated, and it has been actively studied owing to its fertile fundamental physics and potential applications in generating attosecond pulses. HHG was first observed in atomic gases [25–29] and recently in solids such as semiconductors [30–40], topological materials [41–44], and strongly correlated systems [45–67]. Condensed matter systems are promising pulse sources because their density is much higher than that of atomic gas systems, and research on attosecond pulse generation in such systems [33,68–72] has recently been triggered by the development of waveform synthesis of optical electric fields [73–78].

One of the difficulties in shortening the pulse duration lies in a chirp of wave packets. Ionized or excited free electrons (holes) have a positive (negative) mass—i.e., chirp—and their sign does not change. Therefore, the width of the wave packet monotonically spreads out as time evolves, which broadens the pulse width when carriers recombine, as depicted in Fig. 1(a). In atomic gas systems, this issue can be resolved by passing pulses through a metal foil with negative

dispersion, leading to a pulse duration of several tens of attoseconds [79,80]. On the other hand, in crystalline solids, the sign of the effective mass of carriers can be changed by optical driving [see Fig. 1(b)], suggesting an efficient way to refocus wave packets based on the inherent nature of Bloch electrons.

There are two contributions to the pulse emission from solids: intraband currents due to nonlinear changes in carrier velocities, and interband currents associated with recombination of carrier wave packets. Since the nonlinear changes in carrier velocities arise mainly from the Bloch oscillation, the pulse duration can be shortened by increasing the intensity of the external pulses. For example, Ref. [33] reported that in SiO_2, single-cycle optical pulses with a peak strength of $110 \, MV \, cm^{-1}$ drive intraband currents and yield ultrashort pulses with a duration of 472 as. However, common semiconductors are often prone to ablation when subjected to electric fields of several tens of $MV \, cm^{-1}$, which poses a challenge for generating attosecond pulses through intraband currents. In addition, while the spectrum of pulses generated from intraband currents typically spans the extreme ultraviolet to soft x-ray range, there is also a strong desire for ultrashort pulses in the ultraviolet range for application in time-resolved spectroscopy of atoms, molecules, and condensed matter [81–83], which is beginning to be achieved with state-of-the-art optical technology including waveform synthesis [84] and fiber optics [85].

On the other hand, attosecond pulse generation based on interband currents has received mainly theoretical attention [69–71] and still remains elusive because, for instance, the theoretical description of quantum tunneling induced by intense electric fields is difficult [28,80,86–90]. Despite the previous studies, a systematic procedure for optimizing the incident light to achieve the Fourier limit has not been established, which is crucial for generating attosecond pulses covering the ultraviolet range. Recently, a theoretical study [91] analyzed the pulse emission generated by the recombination of resonantly excited carriers. The results of that study imply that if carriers are excited through quantum
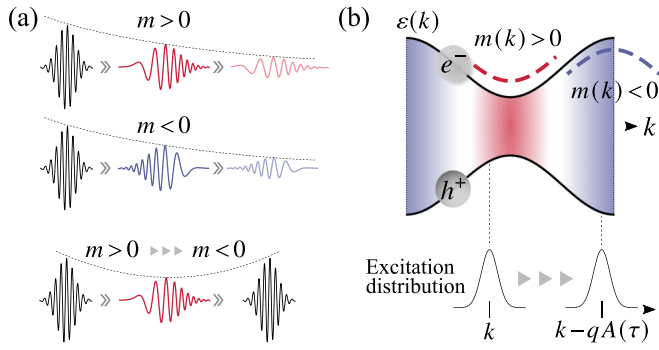
FIG. 1. (a) Dynamics of wave packets in real space. The wave packet of free or undriven particles monotonically spreads out (top two panels), whereas that of Bloch electrons can be refocused by optical driving (bottom panel). (b) Sketch of optically driven particles in crystalline solids. The sign of the effective mass changes during optical driving.

tunneling and subsequently driven by an optical field, their energy spectrum will be broad, and the sign of the carrier mass can be reversed, which may lead to a short pulse width. Furthermore, the emitted pulse spectrum is expected to span the ultraviolet (or even visible) range, depending on the band width and energy gap.

In this Letter, we investigate the real-time dynamics of tunneling electron-hole pairs in an intense electric-field pulse. First, we make an ansatz for the wave function of the tunneling electron-hole pairs by expanding a rigorous formula for quantum tunneling of massive Dirac fermions [92] into that of Bloch electrons in crystalline solids. We then propose a method for optimizing the waveform of a driving pulse to shorten the emitted pulse duration. A numerical simulation successfully demonstrates the generation of a short pulse near the Fourier limit, revealing that the dynamic sign change in the effective mass, which is unique to Bloch electrons, plays an essential role.

Ansatz for the wave function of tunneling particles. Given a conduction band and a valence band involved with quantum tunneling due to an intense pulse, we can consider a two-band effective model described by the Dirac equation

$$(i\partial\!\!\!/ - mv)\psi = 0, \qquad (1)$$

with $\hbar = 1$, where ψ denotes the Dirac spinor for a fermion with mass m, and v is the counterpart of the speed of light. The positive-energy (negative-energy) solution of Eq. (1), denoted by ψ^{cb} (ψ^{vb}), corresponds to the conduction (valence) electron. Narozhnyi and Nikishov [92] derived rigorous expressions for ψ^{cb} and ψ^{vb} after tunneling of electrons induced by the Sauter potential, $A_S(\tau) = -A_{S0}[1 + \tanh(\omega_S\tau)]/2$, where τ represents time. The electric field of the Sauter potential, $E_S(\tau) = -\partial_\tau A_S(\tau) = A_{S0}\omega_S \text{sech}^2(\omega_S\tau)/2$, reaches its peak value of $A_{S0}\omega_S/2$ at $\tau = 0$ and induces electron tunneling.

In this work, we extend the Narozhnyi-Nikishov formula to encompass crystalline band insulators in a vector potential that is not restricted to the Sauter potential, by making an ansatz for the wave function of the tunneling electron-hole pair,

$$\psi_k^{vb}(\tau)^* \psi_k^{cb}(\tau)$$

$$\approx |\psi_k^{vb}||\psi_k^{cb}| \frac{G(\mu + \nu - \lambda)G(-\mu + \nu + \lambda)G(-\mu + \nu - \lambda)}{G(-\mu - \nu - \lambda)G(2\nu)^2}$$

$$\times \exp\left(i \int_0^\infty d\tau \{\varepsilon_D(k - qA_S(\tau)) - \varepsilon_D(k - qA_S(\infty))\}\right)$$

$$\times \exp\left\{-i \int_0^\tau d\tau' \varepsilon(k - qA(\tau'))\right\}, \qquad (2)$$

for $\tau \gtrsim |\omega_S^{-1}|$. Here, $\varepsilon(k)$ represents the energy of the electron-hole pair with momentum k in a band insulator, and $\varepsilon_D(k) = 2\sqrt{(mv^2)^2 + (vk)^2}$ is that for Dirac fermions. The absolute values of the wave functions are given by $|\psi_k^{cb}| = \sqrt{\text{sh}(\mu + \nu - \lambda)\text{sh}(-\mu - \nu - \lambda)/\text{sh}(-2\mu)\text{sh}(2\nu)}$ and $|\psi_k^{vb}| = \sqrt{\text{sh}(-\mu + \nu + \lambda)\text{sh}(-\mu + \nu - \lambda)/\text{sh}(-2\mu)\text{sh}(2\nu)}$, where $\text{sh}(x)$ is shorthand for $\sinh(\pi x)$. The function G is defined by $G(y) = \sqrt{y \sinh(\pi y)/\pi} \Gamma(iy)$ for $y \in \mathbb{R}$ with Γ being the gamma function, satisfying $|G| = 1$. The parameters m and v are given by the relations $mv^2 = \varepsilon(k_0)/2$ and $v^2 = \varepsilon''(k_0)\varepsilon(k_0)/4$, and thereby $\varepsilon(k)$ can be approximated by the Dirac dispersion around each minimum of $\varepsilon(k)$ at $k = k_0$. The other parameters μ, ν, and λ are determined by the relations $2\omega_S\mu = -\varepsilon_D(k)/2$, $2\omega_S\nu = \varepsilon_D(k + qA_{S0})/2$, and $2\omega_S\lambda = -vqA_{S0}$. The electric charge q is set to one in our calculations. Since we are interested in a situation where the electric field $E(\tau) = -\partial_\tau A(\tau)$ has a strong peak that causes electron tunneling, A_{S0} and ω_S are set to $A_{S0} = -2A(0)$ and $\omega_S = -E(0)/A(0)$, with $\tau = 0$ being the time when $E(\tau)$ reaches its maximum. Note that replacing $\varepsilon(k)$ with $\varepsilon_D(k)$ and $A(\tau)$ with $A_S(\tau)$ reproduces the result in Ref. [92]. To achieve attosecond pulse generation without unnecessary complications, we will assume that the tunneling pairs are driven around each minimum of $\varepsilon(k)$ and experience tunneling only once so that Eq. (2) can be applied independently to every tunneling pair around the minimum [93].

Our ansatz in Eq. (2) can describe not only the asymptotic state of the electron-hole pair after quantum tunneling, but also the transient dynamics induced by optical driving, as shown later. The phase factor in the second to last line of Eq. (2) describes the dynamical phase attributed to the backward time evolution of Dirac fermions from time $\tau \to \infty$ to 0, and that in the last line is the dynamical phase of Bloch electrons from time 0 to τ; these are crucial for compensating for the discrepancy between the given dispersion relation $\varepsilon(k)$ and the Dirac dispersion relation $\varepsilon_D(k)$. Furthermore, even though Eq. (2) is deduced from the analytical result for massive Dirac fermions, we can apply it to insulators with indirect band gaps since it involves only the difference between the energies of the conduction and valence bands, $\varepsilon(k)$, and also to two- or three-dimensional systems by considering one-dimensional carrier motions along high-symmetry lines driven by a linearly polarized pulse [91].

Optimization of an optical driving field. To facilitate the analysis, we divide the vector potential of an external optical pulse, A, into two parts: an excitation pulse A_e, which causes quantum tunneling of electrons, and a driving pulse A_d, which drives the electron-hole pairs after tunneling. The excitation

pulse is assumed to have a strong peak at $\tau = 0$, while its waveform can be arbitrary. The driving pulse reverses the relative group velocity of the electron-hole pair, resulting in pair recombination and pulse emission [91]. To minimize the duration of the emitted light pulse by optimizing the waveform of the driving pulse, we consider a set of the vector-potential values at several representative times, $\{A_d(\tau_j)\}_{j=0,1,...,M}$, with $\tau_j = j\delta\tau_d$. We reconstruct $A_d(\tau)$ from $\{A_d(\tau_j)\}$ by performing a fifth-order spline interpolation with boundary conditions: $A_d(\tau_0) = \partial_\tau A_d(\tau_0) = \partial_\tau^2 A_d(\tau_0) = 0$, $A_d(\tau_M) = -A_e(\infty)$ [i.e., $A(\infty) = 0$], and $\partial_\tau A_d(\tau_M) = \partial_\tau^2 A_d(\tau_M) = 0$.

To take advantage of the analytical expression in Eq. (2), we rewrite Eq. (2) as $\psi_k^{vb}(\tau)^* \psi_k^{cb}(\tau) = f_k \exp[i\varphi_k(\tau)]$. Here, $f_k = |\psi_k^{vb}||\psi_k^{cb}|$ represents the amplitude, which is governed by $A_e(\tau)$, and the phase $\varphi_k(\tau)$ is a functional of $A_d(\tau)$. Since the interband electric current is given by $J_{inter}(\tau) = \sum_k J_{k-qA_d(\tau)}^{vc} \psi_k^{vb}(\tau)^* \psi_k^{cb}(\tau) + \text{c.c.}$, with J_k^{vc} being the transition dipole moment [94], the phase of the wave function (and thus that of the electric current), φ_k, should be k independent when the electron and hole recombine at $\tau = \tau_r$, for a minimum pulse duration. We thus employ the Gauss-Newton method to minimize the residual sum of squares (RSS) defined by $R = N_r^{-1} \sum_k \tilde{f}_k^n [\partial_k \varphi_k(\tau_r)]^2$. Here, N_r represents the number of wave numbers used for the optimization, $\tilde{f}_k$ ($\propto f_k$) denotes the normalized weight, and the exponent n of $\tilde{f}_k$ is chosen such that the numerical procedure is kept stable. In our calculations, we used $N_r = 100$ and $n = 14$, and neglected eigenvalues smaller than 10^{-3} when solving the linear equations. The gradient of RSS, $\delta R/\delta A_d(\tau_j)$, is given by the product of $\delta R/\delta A_d(\tau)$ and $\delta A_d(\tau)/\delta A_d(\tau_j)$; the latter derivative can be efficiently evaluated by replacing the spline function for $(A_d(\tau_0), A_d(\tau_1), \ldots, A_d(\tau_M))$ with that for $(0, \ldots, 0, 1, 0, \ldots, 0)$, where only the jth component is one.

Numerical results. To demonstrate the validity of the wave function in Eq. (2) and the effectiveness of our optimization method, we consider a tight-binding model for a band insulator. The Hamiltonian is given by $\mathcal{H} = \sum_k \vec{c}_k^\dagger H_k \vec{c}_k$, with

$$H_k = -2t_h \cos(k)\,\sigma^x - (E_g/2)\,\sigma^z, \qquad (3)$$

where $\vec{c}_k^\dagger = (c_{k1}^\dagger, c_{k2}^\dagger)$ is a vector of creation operators for electrons in orbital $\nu = 1, 2$ with crystal momentum k, and σ^x and σ^z denote the Pauli matrices. The lattice constant a is set to one. The parameters t_h and E_g represent the transfer integral and the energy gap, respectively. We used $t_h = 3$ eV and $E_g = 3$ eV as typical values for the band width (≈ 10 eV) and energy gap of semiconductors such as ZnO. The energy of the electron-hole pair is given by $\varepsilon(k) = 2\sqrt{(2t_h \cos k)^2 + (E_g/2)^2}$, which has two minima at $k = \pm\pi/2$ ($\equiv \pm k_0$) in the first Brillouin zone, resulting in $mv^2 = E_g/2$ and $v = +2t_h$ ($-2t_h$) for $k = +k_0$ ($-k_0$). In this model, it is sufficient to consider only one of the minima at $k = +k_0$ owing to the symmetry of this model; in general, we need to minimize the weighted sum of RSSs for all k_0's [95].

The vector potential $A(\tau)$ is introduced through the Peierls substitution, $k \mapsto k - qA(\tau)$. In particular, we chose an excitation pulse given by $A_e(\tau) = -A_{e0}[1 + \text{erf}(\omega_e \tau/\sqrt{2})]/2$, where erf is the error function, for which the Sauter-potential parameters are $A_{S0} = A_{e0}$ and $\omega_S = \omega_e \sqrt{2/\pi}$; we used $A_{e0} = \pi/2$ and $\omega_e = 0.2t_h$ so that the excitation
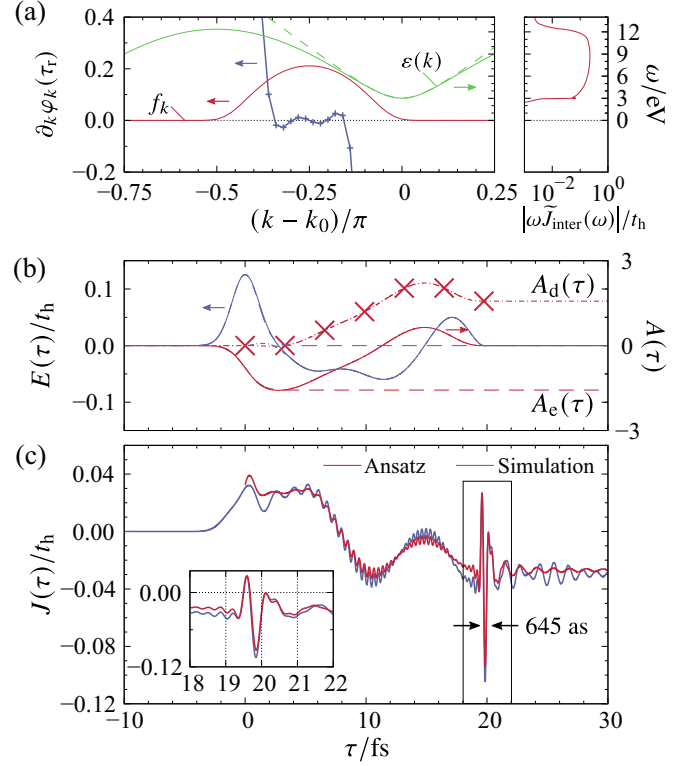

FIG. 2. (a) Left panel: optimized phase derivative at recombination time, $\tau_r \approx 20$ fs (blue points), and excitation distribution f_k (red curve). The green and dashed-green curves represent the dispersion relations of the tight-binding model and the Dirac fermions, respectively. Right panel: the Fourier spectrum $\tilde{J}_{inter}(\omega)$ of the interband current for $\tau \geqslant 17.1$ fs multiplied by ω. (b) Optimized waveforms of the electric field (blue curve) and vector potential (red curves). The crosses indicate the representatives $\{A_d(\tau_j)\}$ used for optimization. (c) Electric currents calculated from the ansatz (red) and from the numerical simulation (blue). The inset is an enlarged view from $\tau = 18$ to 22 fs.

distribution would be broad in energy. The time evolution of the state $|\Psi(\tau)\rangle$ is described by $|\Psi(\tau + \delta\tau)\rangle = \exp[-i\mathcal{H}(\tau + \delta\tau/2)\delta\tau]|\Psi(\tau)\rangle + \mathcal{O}(\delta\tau^3)$. The electric current is defined by $J(\tau) = \langle\Psi(\tau)|\hat{J}(\tau)|\Psi(\tau)\rangle$, with $\hat{J}(\tau) = -N^{-1}\delta\mathcal{H}(\tau)/\delta A(\tau)$, where N represents the number of k points. We employ $\tau_r = 90t_h^{-1} \approx 20$ fs, $\delta\tau_d = 15t_h^{-1}$, and $M = 6$ for the optimization, and $\delta\tau = 0.03t_h^{-1}$ and $N = 1000$ for the simulation. We set $t_h/(qa) = 92$ MV cm^{-1} and $qt_h/\hbar = 0.73$ mA as the units of the electric fields and electric currents, respectively, for $t_h = 3$ eV and $a = 3.25$ Å.

The left panel of Fig. 2(a) shows the excitation distribution of the electron-hole pair, f_k, and the optimized phase derivative, $\partial_k \varphi_k$, at time $\tau = \tau_r$. The phase derivative was successfully optimized, i.e., $\partial_k \varphi_k \approx 0$, around the center of the excitation distribution, $k - k_0 = k_c = -qA_{S0}/2 = -\pi/4$, with $R = 2.18 \times 10^{-5}$. The optimized waveforms of the electric field and vector potential are plotted in Fig. 2(b), where we took seven representatives $\{A_d(\tau_j)\}_{j=0,1,...,6}$ as indicated by the crosses. Figure 2(c) displays the electric current calculated from our ansatz in Eq. (2) and that from the numerical simulation of the tight-binding model. The electric field reaches its
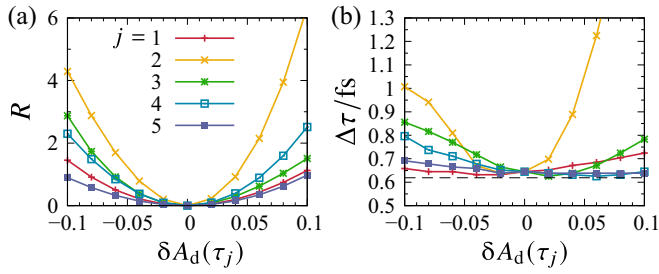
FIG. 3. (a) RSS as a function of $\delta A_\mathrm{d}(\tau_j)$. (b) FWHM of the generated pulse. The dashed line indicates the Fourier-limited pulse duration.

maximum at $\tau = 0$, and the electric current associated with the tunneling particles flows simultaneously. Following the optical driving, a subcycle electric current pulse is generated at $\tau \approx 20$ fs with an emission spectrum in the ultraviolet range, as shown in the right panel of Fig. 2(a). The full width at half maximum (FWHM) of the pulse envelope obtained from the Hilbert transformation is 645 as. There is good agreement between the ansatz and the numerical simulation, which indicates that the wave function in Eq. (2) can accurately describe not only the asymptotic state in the long-time limit, but also the transient state under optical driving.

Figure 3 shows the effects of an error in the representative $A_\mathrm{d}(\tau_j)$ on the RSS, R, and the FWHM of the generated pulse calculated from the ansatz, $\Delta\tau$, when one of the representatives deviates from the optimized value $A_\mathrm{d}(\tau_j)$ to $A_\mathrm{d}(\tau_j) + \delta A_\mathrm{d}(\tau_j)$. The RSS grows quadratically with $\delta A_\mathrm{d}(\tau_j)$, indicating that the optimization procedure was successfully performed. Furthermore, we find in Fig. 3(b) that the FWHM of the optimized pulse is close to the Fourier limit (≈ 619 as), which is evaluated by replacing $\psi_k^{\mathrm{vb}*}\psi_k^{\mathrm{cb}}$ with $f_k \exp[-i\varepsilon(k)(\tau - \tau_\mathrm{r})]$, and is rather insensitive to $\delta A_\mathrm{d}(\tau_j)$ [96]. If one needs to generate a pulse with a FWHM less than 1 fs, the allowable error in the vector potential is estimated to be $|\delta A(\tau_j)/A(\tau_j)| \lesssim 0.03$ for $\tau = \tau_{j=2}$.

Discussion. To gain insight into the underlying mechanism of the short-pulse generation demonstrated above, let us consider a case where only two parameters—e.g., τ_r and $A_\mathrm{d}(\tau_1)$ when $M = 2$—are optimized. In this case, the condition that R is minimized can be written as

$$\partial_k \varphi_k(\tau_\mathrm{r})|_{k=k_\mathrm{c}} = 0, \qquad (4)$$

$$\partial_k^2 \varphi_k(\tau_\mathrm{r})|_{k=k_\mathrm{c}} = 0, \qquad (5)$$

where we set $k_0 = 0$ for simplicity. Since $\varphi_k(\tau_\mathrm{r})$ can be expressed as $\varphi_k(\tau) = \theta_k - \int_0^\tau \mathrm{d}\tau' \, \varepsilon(k - qA(\tau'))$, with θ_k being a time-independent constant, Eq. (4) reduces to $-\partial_k \theta_k|_{k=k_\mathrm{c}} + \int_0^{\tau_\mathrm{r}} \mathrm{d}\tau \, \partial_k \varepsilon(k - qA(\tau))|_{k=k_\mathrm{c}} = 0$, which means that the relative displacement between the electron and hole is zero at $\tau = \tau_\mathrm{r}$, given that $-\partial_k \theta_k|_{k=k_\mathrm{c}}$ corresponds to the relative displacement at $\tau = 0$ as discussed in Refs. [28,89,97–99].

Equation (5) states that the chirp of the wave packet of the electron-hole pair is zero at $\tau = \tau_\mathrm{r}$, and it can be written as $\int_0^{\tau_\mathrm{r}} \mathrm{d}\tau \, m^{-1}(k - qA(\tau))|_{k=k_\mathrm{c}} = \partial_k^2 \theta_k|_{k=k_\mathrm{c}}$, where

$m^{-1}(k) = \partial_k^2 \varepsilon(k)$ denotes the inverse mass. The right-hand side is a constant with an approximate value of 0.57 in the present calculation. On the other hand, for massive Dirac fermions with $m_\mathrm{D}^{-1}(k) = \partial_k^2 \varepsilon_\mathrm{D}(k) > 0$, the time integral of the inverse mass monotonically increases and is estimated to be of the order of 10^2; therefore, the condition in Eq. (5) is not satisfied. As a result, the wave packet of free particles gradually spreads out in real space [the top two panels of Fig. 1(a)]. In crystalline solids, however, the sign of the effective mass can change during optical driving, as depicted in Fig. 1(b), which enables a reduction in the pulse duration by refocusing the wave packet [the bottom panel of Fig. 1(a)]. The video in the Supplemental Material [94] illustrates this real-space motion of the wave packet.

According to the semiclassical analysis based on the three-step model, the recombination at $\tau \approx 20$ fs is attributed to electrons following a long trajectory [94]. The driving field controls the chirp of this long trajectory through the dynamic sign change in the effective mass. Consequently, the Fourier-limited pulses can be generated from the entire current without, e.g., filtering harmonics [29].

Finally, let us discuss the effect of dephasing on the short-pulse generation. Since the fastest timescale of dephasing or relaxation in solids is typically of the order of ten femtoseconds, the coherence of electrons must be maintained on that timescale to observe intriguing ultrafast phenomena. If we consider a dephasing time T_2 independent of the wave numbers of the carriers, the interband current will decay exponentially as $J(\tau) \propto \exp(-\tau/T_2)$ [100], while its waveform—i.e., pulse duration—remains unchanged. However, a more profound study that explicitly considers dephasing will be left for future work.

Conclusion. We demonstrated that attosecond pulses can be generated by controlling the motion of tunneling particles in solids by using optical driving. The ansatz for the wave function of tunneling particles in Eq. (2) facilitates efficient optimization of the optical driving pulse, resulting in a substantial reduction in the pulse duration towards the Fourier limit. The central frequency of the emitted pulse lies in the ultraviolet range and could potentially be reduced to the visible range, depending on the band gap. The intensity of the external electric-field pulse ($\sim 0.1 t_\mathrm{h}$) is of the order of several MV cm^{-1}, which is one or two orders of magnitude smaller than that based on the intraband current mechanism. The present results provide a theoretical limit for the pulse duration and suggest that semiconductors with wide energy bandwidths and broad negative-mass regions are promising sources of attosecond light pulses in combination with waveform synthesis [73–78] of optical electric fields, specifically in the mid- to near-infrared range.

[1] D. Strickland, Nobel Lecture: Generating high-intensity ultrashort optical pulses, Rev. Mod. Phys. **91**, 030502 (2019).

[2] G. Mourou, Nobel Lecture: Extreme light physics and application, Rev. Mod. Phys. **91**, 030501 (2019).

[3] A. H. Zewail, Laser femtochemistry, Science **242**, 1645 (1988).

[4] S. Koshihara, T. Ishikawa, Y. Okimoto, K. Onda, R. Fukaya, M. Hada, Y. Hayashi, S. Ishihara, and T. Luty, Challenges for developing photo-induced phase transition (PIPT) systems: From classical (incoherent) to quantum (coherent) control of PIPT dynamics, Phys. Rep. **942**, 1 (2022).

[5] S. Ishihara, Photoinduced ultrafast phenomena in correlated electron magnets, J. Phys. Soc. Jpn. **88**, 072001 (2019).

[6] T. Miyamoto, H. Yamakawa, T. Morimoto, and H. Okamoto, Control of electronic states by a nearly monocyclic terahertz electric-field pulse in organic correlated electron materials, J. Phys. B **51**, 162001 (2018).

[7] A. Kirilyuk, A. V. Kimel, and T. Rasing, Ultrafast optical manipulation of magnetic order, Rev. Mod. Phys. **82**, 2731 (2010).

[8] P. Agostini and L. F. DiMauro, The physics of attosecond light pulses, Rep. Prog. Phys. **67**, 813 (2004).

[9] F. Krausz and M. Ivanov, Attosecond physics, Rev. Mod. Phys. **81**, 163 (2009).

[10] L. Gallmann, C. Cirelli, and U. Keller, Attosecond science: Recent highlights and future trends, Annu. Rev. Phys. Chem. **63**, 447 (2012).

[11] D. T. Reid, C. M. Heyl, R. R. Thomson, R. Trebino, G. Steinmeyer, H. H. Fielding, R. Holzwarth, Z. Zhang, P. Del'Haye, T. Südmeyer, G. Mourou, T. Tajima, D. Faccio, F. J. M. Harren, and G. Cerullo, Roadmap on ultrafast optics, J. Opt. **18**, 093006 (2016).

[12] K. Ramasesha, S. R. Leone, and D. M. Neumark, Real-time probing of electron dynamics using attosecond time-resolved spectroscopy, Annu. Rev. Phys. Chem. **67**, 41 (2016).

[13] J. Li, J. Lu, A. Chew, S. Han, J. Li, Y. Wu, H. Wang, S. Ghimire, and Z. Chang, Attosecond science based on high harmonic generation from gases and solids, Nat. Commun. **11**, 2748 (2020).

[14] G. Pitruzzello, A bright future for attosecond physics, Nat. Photon. **16**, 550 (2022).

[15] E. Goulielmakis, V. S. Yakovlev, A. L. Cavalieri, M. Uiberacker, V. Pervak, A. Apolonski, R. Kienberger, U. Kleineberg, and F. Krausz, Attosecond control and measurement: Lightwave electronics, Science **317**, 769 (2007).

[16] F. Krausz and M. I. Stockman, Attosecond metrology: From electron capture to future signal processing, Nat. Photon. **8**, 205 (2014).

[17] T. T. Luu, M. Garg, S. Y. Kruchinin, A. Moulet, M. T. Hassan, and E. Goulielmakis, Extreme ultraviolet high-harmonic spectroscopy of solids, Nature (London) **521**, 498 (2015).

[18] J. Reimann, S. Schlauderer, C. P. Schmid, F. Langer, S. Baierl, K. A. Kokh, O. E. Tereshchenko, A. Kimura, C. Lange, J. Güdde, U. Höfer, and R. Huber, Subcycle observation of lightwave-driven Dirac currents in a topological surface band, Nature (London) **562**, 396 (2018).

[19] Y. Kawakami, H. Itoh, K. Yonemitsu, and S. Iwai, Strong light-field effects driven by nearly single-cycle 7 fs

light-field in correlated organic conductors, J. Phys. B **51**, 174005 (2018).

[20] Y. Kawakami, T. Amano, Y. Yoneyama, Y. Akamine, H. Itoh, G. Kawaguchi, H. M. Yamamoto, H. Kishida, K. Itoh, T. Sasaki, S. Ishihara, Y. Tanaka, K. Yonemitsu, and S. Iwai, Nonlinear charge oscillation driven by a single-cycle light field in an organic superconductor, Nat. Photon. **12**, 474 (2018).

[21] J. Schoetz, Z. Wang, E. Pisanty, M. Lewenstein, M. F. Kling, and M. F. Ciappina, Perspective on petahertz electronics and attosecond nanoscopy, ACS Photon. **6**, 3057 (2019).

[22] Y. Kawakami, T. Amano, H. Ohashi, H. Itoh, Y. Nakamura, H. Kishida, T. Sasaki, G. Kawaguchi, H. M. Yamamoto, K. Yamamoto, S. Ishihara, K. Yonemitsu, and S. Iwai, Petahertz nonlinear current in a centrosymmetric organic superconductor, Nat. Commun. **11**, 4138 (2020).

[23] Á. Jiménez-Galán, R. E. F. Silva, O. Smirnova, and M. Ivanov, Subcycle valleytronics: Control of valley polarization using few-cycle linearly polarized pulses, Optica **8**, 277 (2021).

[24] T. Boolakee, C. Heide, A. Garzón-Ramírez, H. B. Weber, I. Franco, and P. Hommelhoff, Light-field control of real and virtual charge carriers, Nature (London) **605**, 251 (2022).

[25] A. McPherson, G. Gibson, H. Jara, U. Johann, T. S. Luk, I. A. McIntyre, K. Boyer, and C. K. Rhodes, Studies of multiphoton production of vacuum-ultraviolet radiation in the rare gases, J. Opt. Soc. Am. B **4**, 595 (1987).

[26] M. Ferray, A. L'Huillier, X. F. Li, L. A. Lompre, G. Mainfray, and C. Manus, Multiple-harmonic conversion of 1064 nm radiation in rare gases, J. Phys. B **21**, L31 (1988).

[27] P. B. Corkum, Plasma perspective on strong field multiphoton ionization, Phys. Rev. Lett. **71**, 1994 (1993).

[28] M. Lewenstein, P. Balcou, M. Y. Ivanov, A. L'Huillier, and P. B. Corkum, Theory of high-harmonic generation by low-frequency laser fields, Phys. Rev. A **49**, 2117 (1994).

[29] M. Hentschel, R. Kienberger, C. Spielmann, G. A. Reider, N. Milosevic, T. Brabec, P. Corkum, U. Heinzmann, M. Drescher, and F. Krausz, Attosecond metrology, Nature (London) **414**, 509 (2001).

[30] S. Ghimire, A. D. DiChiara, E. Sistrunk, P. Agostini, L. F. DiMauro, and D. A. Reis, Observation of high-order harmonic generation in a bulk crystal, Nat. Phys. **7**, 138 (2011).

[31] O. Schubert, M. Hohenleutner, F. Langer, B. Urbanek, C. Lange, U. Huttner, D. Golde, T. Meier, M. Kira, S. W. Koch, and R. Huber, Subcycle control of terahertz high-harmonic generation by dynamical Bloch oscillations, Nat. Photon. **8**, 119 (2014).

[32] M. Hohenleutner, F. Langer, O. Schubert, M. Knorr, U. Huttner, S. W. Koch, M. Kira, and R. Huber, Real-time observation of interfering crystal electrons in high-harmonic generation, Nature (London) **523**, 572 (2015).

[33] M. Garg, M. Zhan, T. T. Luu, H. Lakhotia, T. Klostermann, A. Guggenmos, and E. Goulielmakis, Multi-petahertz electronic metrology, Nature (London) **538**, 359 (2016).

[34] F. Langer, M. Hohenleutner, C. P. Schmid, C. Poellmann, P. Nagler, T. Korn, C. Schüller, M. S. Sherwin, U. Huttner, J. T. Steiner, S. W. Koch, M. Kira, and R. Huber,

Lightwave-driven quasiparticle collisions on a subcycle timescale, Nature (London) **533**, 225 (2016).

[35] F. Langer, M. Hohenleutner, U. Huttner, S. W. Koch, M. Kira, and R. Huber, Symmetry-controlled temporal structure of high-harmonic carrier fields from a bulk crystal, Nat. Photon. **11**, 227 (2017).

[36] U. Huttner, M. Kira, and S. W. Koch, Ultrahigh off-resonant field effects in semiconductors, Laser Photon. Rev. **11**, 1700049 (2017).

[37] S. Y. Kruchinin, F. Krausz, and V. S. Yakovlev, Colloquium: Strong-field phenomena in periodic systems, Rev. Mod. Phys. **90**, 021002 (2018).

[38] L. Ortmann and A. S. Landsman, High-harmonic generation in solids, in *Advances In Atomic, Molecular, and Optical Physics*, 1st ed. (Academic Press, United States, 2021), Vol. 70, pp. 103–156.

[39] P. Xia, T. Tamaya, C. Kim, F. Lu, T. Kanai, N. Ishii, J. Itatani, H. Akiyama, and T. Kato, High-harmonic generation in GaAs beyond the perturbative regime, Phys. Rev. B **104**, L121202 (2021).

[40] T. Tamaya, A. Ishikawa, T. Ogawa, and K. Tanaka, Diabatic mechanisms of higher-order harmonic generation in solid-state materials under high-intensity electric fields, Phys. Rev. Lett. **116**, 016601 (2016).

[41] N. Yoshikawa, T. Tamaya, and K. Tanaka, High-harmonic generation in graphene enhanced by elliptically polarized light excitation, Science **356**, 736 (2017).

[42] Y. Bai, F. Fei, S. Wang, N. Li, X. Li, F. Song, R. Li, Z. Xu, and P. Liu, High-harmonic generation from topological surface states, Nat. Phys. **17**, 311 (2021).

[43] C. P. Schmid, L. Weigl, P. Grössing, V. Junk, C. Gorini, S. Schlauderer, S. Ito, M. Meierhofer, N. Hofmann, D. Afanasiev, J. Crewse, K. A. Kokh, O. E. Tereshchenko, J. Güdde, F. Evers, J. Wilhelm, K. Richter, U. Höfer, and R. Huber, Tunable non-integer high-harmonic generation in a topological insulator, Nature (London) **593**, 385 (2021).

[44] Y.-y. Lv, J. Xu, S. Han, C. Zhang, Y. Han, J. Zhou, S.-h. Yao, X.-p. Liu, M.-h. Lu, H. Weng, Z. Xie, Y. B. Chen, J. Hu, Y.-f. Chen, and S. Zhu, High-harmonic generation in Weyl semimetal β-WP$_2$ crystals, Nat. Commun. **12**, 6437 (2021).

[45] R. E. F. Silva, I. V. Blinov, A. N. Rubtsov, O. Smirnova, and M. Ivanov, High-harmonic spectroscopy of ultrafast many-body dynamics in strongly correlated systems, Nat. Photon. **12**, 266 (2018).

[46] Y. Murakami, M. Eckstein, and P. Werner, High-harmonic generation in mott insulators, Phys. Rev. Lett. **121**, 057405 (2018).

[47] N. Tancogne-Dejean, M. A. Sentef, and A. Rubio, Ultrafast modification of hubbard U in a strongly correlated material: *Ab initio* high-harmonic generation in NiO, Phys. Rev. Lett. **121**, 097402 (2018).

[48] T. Nag, R.-J. Slager, T. Higuchi, and T. Oka, Dynamical synchronization transition in interacting electron systems, Phys. Rev. B **100**, 134301 (2019).

[49] A. Roy, S. Bera, and K. Saha, Nonlinear dynamical response of interacting bosons to synthetic electric field, Phys. Rev. Res. **2**, 043133 (2020).

[50] Y. Murakami, S. Takayoshi, A. Koga, and P. Werner, High-harmonic generation in one-dimensional Mott insulators, Phys. Rev. B **103**, 035110 (2021).

[51] M. S. Mrudul, Á. Jiménez-Galán, M. Ivanov, and G. Dixit, Light-induced valleytronics in pristine graphene, Optica **8**, 422 (2021).

[52] M. S. Mrudul and G. Dixit, High-harmonic generation from monolayer and bilayer graphene, Phys. Rev. B **103**, 094308 (2021).

[53] C. Orthodoxou, A. Zaïr, and G. H. Booth, High harmonic generation in two-dimensional Mott insulators, npj Quantum Mater. **6**, 76 (2021).

[54] M. Udono, K. Sugimoto, T. Kaneko, and Y. Ohta, Excitonic effects on high-harmonic generation in Mott insulators, Phys. Rev. B **105**, L241108 (2022).

[55] C. Shao, H. Lu, X. Zhang, C. Yu, T. Tohyama, and R. Lu, High-harmonic generation approaching the quantum critical point of strongly correlated systems, Phys. Rev. Lett. **128**, 047401 (2022).

[56] M. Lysne, Y. Murakami, and P. Werner, Signatures of bosonic excitations in high-harmonic spectra of Mott insulators, Phys. Rev. B **101**, 195139 (2020).

[57] S. Imai, A. Ono, and S. Ishihara, High harmonic generation in a correlated electron system, Phys. Rev. Lett. **124**, 157404 (2020).

[58] W. Zhu, B. Fauseweh, A. Chacon, and J.-X. Zhu, Ultrafast laser-driven many-body dynamics and Kondo coherence collapse, Phys. Rev. B **103**, 224305 (2021).

[59] B. Fauseweh and J.-X. Zhu, Laser pulse driven control of charge and spin order in the two-dimensional Kondo lattice, Phys. Rev. B **102**, 165128 (2020).

[60] S. Takayoshi, Y. Murakami, and P. Werner, High-harmonic generation in quantum spin systems, Phys. Rev. B **99**, 184303 (2019).

[61] M. Kanega, T. N. Ikeda, and M. Sato, Linear and nonlinear optical responses in Kitaev spin liquids, Phys. Rev. Res. **3**, L032024 (2021).

[62] M. R. Bionta, E. Haddad, A. Leblanc, V. Gruson, P. Lassonde, H. Ibrahim, J. Chaillou, N. Émond, M. R. Otto, Á. Jiménez-Galán, R. E. F. Silva, M. Ivanov, B. J. Siwick, M. Chaker, and F. Légaré, Tracking ultrafast solid-state dynamics using high harmonic spectroscopy, Phys. Rev. Res. **3**, 023250 (2021).

[63] K. Uchida, G. Mattoni, S. Yonezawa, F. Nakamura, Y. Maeno, and K. Tanaka, High-order harmonic generation and its unconventional scaling law in the Mott-insulating Ca$_2$RuO$_4$, Phys. Rev. Lett. **128**, 127401 (2022).

[64] A. Pattanayak, S. Pujari, and G. Dixit, Role of Majorana fermions in high-harmonic generation from Kitaev chain, Sci. Rep. **12**, 6722 (2022).

[65] Y. Murakami, K. Uchida, A. Koga, K. Tanaka, and P. Werner, Anomalous temperature dependence of high-harmonic generation in mott insulators, Phys. Rev. Lett. **129**, 157401 (2022).

[66] O. Grånäs, I. Vaskivskyi, X. Wang, P. Thunström, S. Ghimire, R. Knut, J. Söderström, L. Kjellsson, D. Turenne, R. Y. Engel, M. Beye, J. Lu, D. J. Higley, A. H. Reid, W. Schlotter, G. Coslovich, M. Hoffmann, G. Kolesov, C. Schüßler-Langeheine, A. Styervoyedov *et al.*, Ultrafast modification of the electronic structure of a correlated insulator, Phys. Rev. Res. **4**, L032030 (2022).

[67] J. Alcalà, U. Bhattacharya, J. Biegert, M. Ciappina, U. Elu, T. Graß, P. T. Grochowski, M. Lewenstein, A. Palau, T. P. H.

Sidiropoulos, T. Steinle, and I. Tyulnev, High-harmonic spectroscopy of quantum phase transitions in a high-Tc superconductor, Proc. Natl. Acad. Sci. USA **119**, e2207766119 (2022).

[68] M. Garg, H. Y. Kim, and E. Goulielmakis, Ultimate waveform reproducibility of extreme-ultraviolet pulses by high-harmonic generation in quartz, Nat. Photon. **12**, 291 (2018).

[69] Z. Guan, X.-X. Zhou, and X.-B. Bian, High-order-harmonic generation from periodic potentials driven by few-cycle laser pulses, Phys. Rev. A **93**, 033852 (2016).

[70] X. Song, R. Zuo, S. Yang, P. Li, T. Meier, and W. Yang, Attosecond temporal confinement of interband excitation by intraband motion, Opt. Express **27**, 2225 (2019).

[71] Z. Nourbakhsh, N. Tancogne-Dejean, H. Merdji, and A. Rubio, High harmonics and isolated attosecond pulses from MgO, Phys. Rev. Appl. **15**, 014013 (2021).

[72] A. Sadeghifaraz, E. Irani, and M. Monfared, Efficient attosecond pulse generation from WS_2 semiconductor by tailoring the driving laser pulse, Opt. Commun. **516**, 128226 (2022).

[73] M. T. Hassan, A. Wirth, I. Grguraš, A. Moulet, T. T. Luu, J. Gagnon, V. Pervak, and E. Goulielmakis, Invited Article: Attosecond photonics: Synthesis and control of light transients, Rev. Sci. Instrum. **83**, 111301 (2012).

[74] O. D. Mucke, S. Fang, G. Cirmi, G. M. Rossi, S.-H. Chia, H. Ye, Y. Yang, R. Mainz, C. Manzoni, P. Farinello, G. Cerullo, and F. X. Kartner, Toward waveform nonlinear optics using multimillijoule sub-cycle waveform synthesizers, IEEE J. Sel. Top. Quantum Electron. **21**, 1 (2015).

[75] Y.-C. Lin, Y. Nabekawa, and K. Midorikawa, Optical parametric amplification of sub-cycle shortwave infrared pulses, Nat. Commun. **11**, 3413 (2020).

[76] K. Tian, L. He, X. Yang, and H. Liang, Mid-infrared few-cycle pulse generation and amplification, Photonics **8**, 290 (2021).

[77] H. Alqattan, D. Hui, V. Pervak, and M. T. Hassan, Attosecond light field synthesis, APL Photon. **7**, 041301 (2022).

[78] Y. Su, S. Fang, S. Wang, Y. Liang, G. Chang, X. He, and Z. Wei, Optimal generation of delay-controlled few-cycle pulses for high harmonic generation in solids, Appl. Phys. Lett. **120**, 121105 (2022).

[79] T. Gaumnitz, A. Jain, Y. Pertot, M. Huppert, I. Jordan, F. Ardana-Lamas, and H. J. Wörner, Streaking of 43-attosecond soft-x-ray pulses generated by a passively CEP-stable mid-infrared driver, Opt. Express **25**, 27506 (2017).

[80] D. Shafir, H. Soifer, B. D. Bruner, M. Dagan, Y. Mairesse, S. Patchkovskii, M. Y. Ivanov, O. Smirnova, and N. Dudovich, Resolving the time when an electron exits a tunnelling barrier, Nature (London) **485**, 343 (2012).

[81] U. Graf, M. Fieß, M. Schultze, R. Kienberger, F. Krausz, and E. Goulielmakis, Intense few-cycle light pulses in the deep ultraviolet, Opt. Express **16**, 18956 (2008).

[82] M. Galli, V. Wanie, D. P. Lopes, E. P. Månsson, A. Trabattoni, L. Colaizzi, K. Saraswathula, A. Cartella, F. Frassetto, L. Poletto, F. Légaré, S. Stagira, M. Nisoli, R. Martínez Vázquez, R. Osellame, and F. Calegari, Generation of deep ultraviolet sub-2-fs pulses, Opt. Lett. **44**, 1308 (2019).

[83] E. Goulielmakis and T. Brabec, High harmonic generation in condensed matter, Nat. Photon. **16**, 411 (2022).

[84] M. T. Hassan, T. T. Luu, A. Moulet, O. Raskazovskaya, P. Zhokhov, M. Garg, N. Karpowicz, A. M. Zheltikov, V. Pervak, F. Krausz, and E. Goulielmakis, Optical attosecond pulses and tracking the nonlinear response of bound electrons, Nature (London) **530**, 66 (2016).

[85] J. C. Travers, T. F. Grigorova, C. Brahms, and F. Belli, High-energy pulse self-compression and ultraviolet generation through soliton dynamics in hollow capillary fibres, Nat. Photon. **13**, 547 (2019).

[86] N. V. Vitanov and B. M. Garraway, Landau-Zener model: Effects of finite coupling duration, Phys. Rev. A **53**, 4288 (1996).

[87] T. Oka, Nonlinear doublon production in a Mott insulator: Landau-Dykhne method applied to an integrable model, Phys. Rev. B **86**, 075148 (2012).

[88] L. A. MacColl, Note on the transmission and reflection of wave packets by potential barriers, Phys. Rev. **40**, 621 (1932).

[89] E. Yakaboylu, M. Klaiber, and K. Z. Hatsagortsyan, Wigner time delay for tunneling ionization via the electron propagator, Phys. Rev. A **90**, 012116 (2014).

[90] A. S. Kheifets, The attoclock and the tunneling time debate, J. Phys. B **53**, 072001 (2020).

[91] S. Imai, A. Ono, and S. Ishihara, Energy-band echoes: Time-reversed light emission from optically driven quasiparticle wave packets, Phys. Rev. Res. **4**, 043155 (2022).

[92] N. B. Narozhnyi and A. I. Nikishov, The simplest processes in the pair-creating electric field, Sov. J. Nucl. Phys. **11**, 596 (1970).

[93] If the optical field is strong enough to drive electrons over several Brillouin zones, tunneling occurs multiple times as electrons pass through the minima of energy bands. In such cases, one should consider the interference between each tunneling event beyond Eq. (2). However, this scenario is not advantageous for generating attosecond pulses since the optical field strength would be much greater than that considered here, and nevertheless the energy width of the excitation distribution remains nearly the same as the single tunneling case.

[94] See Supplemental Material at http://link.aps.org/supplemental/10.1103/PhysRevB.109.L041303 for a video of the real-space wave-packet motion and for discussions on the emission spectrum, multiband systems, and relation to semiclassical analysis.

[95] According to the Landau-Zener formula, the tunneling probability exponentially decays as the energy gap increases. Therefore, in practice, it would be sufficient to consider one (or a few) of the minima. Our approach is also applicable to multiband systems, as discussed in the Supplemental Material [94].

[96] The minimum FWHM (≈ 625 as) is located away from $\delta A_d = 0$ because we used the same τ_r for $|\delta A_d| \neq 0$.

[97] M. Geissler, G. Tempea, A. Scrinzi, M. Schnürer, F. Krausz, and T. Brabec, Light propagation in field-ionizing media: Extreme nonlinear optics, Phys. Rev. Lett. **83**, 2930 (1999).

[98] P. Jürgens, B. Liewehr, B. Kruse, C. Peltz, D. Engel, A. Husakou, T. Witting, M. Ivanov, M. J. J. Vrakking, T. Fennel, and A. Mermillod-Blondin, Origin of strong-field-induced

low-order harmonic generation in amorphous quartz, Nat. Phys. **16**, 1035 (2020).

[99] G. Wang and T.-Y. Du, Quantum decoherence in high-order harmonic generation from solids, Phys. Rev. A **103**, 063109 (2021).

[100] G. Vampa, C. R. McDonald, G. Orlando, D. D. Klug, P. B. Corkum, and T. Brabec, Theoretical analysis of high-harmonic generation in solids, Phys. Rev. Lett. **113**, 073901 (2014).